Supplementary information for *Angle Sensing in Magnetotaxis of Magnetospirillum magneticum AMB-1*

SI materials and methods

Construction of mutant and complementary strains. About 701 bp upstream of *amb0995* and 700 bp downstream region of *amb0994* were amplified from chromosome and ligated flanked the coding sequence of gentamycin marker gene in pAK1[1]. The resultant plasmid used for homologous recombination was conjugated into wild type *Magnetospirillum magneticum* AMB-1 by the donor strain *Escherichia coli* WM3064. Colonies resistant to gentamycin were further screened for kanamycin sensitivity to obtain the Δ*amb0994-0995* mutant strain.

For verifying Δ*amb0994-0995* mutant strain, we amplified the region adjacent to the genes with the primers at the locus of 1624 bp upstream of *amb0995* and 1420 bp downstream of *amb0994*. The two primers (Table S1) matched well with the expected regions and had no similarity to anywhere in the chromosome. As we expected, the PCR product from mutant stain was about 1000 bp shorter than that from wild type (Fig. S10). Then the PCR products were sequenced for checking whether *amb0994-0995* was replaced by gentamycin marker precisely while leaving the flanking sequences intact.

Insertion mutagenesis was used to disrupt the gene *amb2196*. Briefly, an internal fragment of Amb2196 coding sequence was amplified and ligated into pAK0 generating pAK0-2196[2]. The plasmid was also transconjugated into wild type strain to create Δ*amb2196*. Anchored PCR was performed to confirm that the target gene was inserted with the plasmid (Fig. S10).

For checking the maintenance of the magnetosome island (MAI) in each mutant strain, four makers within MAI were amplified using primer pairs denoted in Fig. S11. Since

four representative segments can be amplified (Fig.S11) in all mutants and wild type strains, the MAI were maintained and the behaviors were indeed due to deleted genes rather than lacking or rearrangement of MAI.

For complementation of *amb0994-0995* (C*amb0994-0995*), full length of *amb0994-0995* with its own promoter were amplified and constructed into pBBR1MCS-5. The resultant plasmid was conjugated into Δ*amb0994-0995* strain.

Preparing vigorous swimming cells. In all motility assays, cells of wild type, mutant and complementation were applied to geomagnetic field[3] and conducted no bias separation for 10 min to obtain the most vigorous cells[3].

Detection of bacteria growth and magnetism

M. magneticum AMB-1 was cultured at 28℃ in an enriched Magnetospirillum growth medium (EMSGM)[4]. Briefly, for investigating the growth and magnetism, strains were inoculated into stoppered 300 mL serum bottles containing 250 mL of culture medium without any aeration and agitation and kept statically, the dissolved oxygen in the medium will be gradually dropped to a microaerobic condition due to bacteria growth[5]. C_{mag} values were measured to account for the magnetism using magneto-spectrophotometer as described previously[6] and the external magnetic field used was 10mT.

Transmission Electron Microscopy (TEM). *M. magneticum* cells grown to early stationary phase were collected, washed twice with ddH_2O, and adsorbed onto carbon-coated copper grids. The transmission images of the cells were performed with tecnai F30 at acceleration voltage of 120 kV. The average magnetosome number per cell was determined directly by counting magnetosome particles in at least 100 individual cells.

Microfluidic device and calibration. Since high concentration of dissolved oxygen

is harmful and lethal to anaerobic AMB-1 but low concentration is required for its growth, we designed the device that can control the O2 concentration on chip as well as establish a concentration gradient to test the aerotaxis behavior. The mold of our chips were fabricated using standard photolithography[7]. As shown in Fig.S9, the observation window was designed 400μm×400 μm to fit the field of view using 20X objective lens and fabricated to be 25μm in height considering both the depth of field and the swimming of bacteria. The gas channel has the width of 300μm and height of 25μm. The distance between gas channel and boundary of observation window is 40μm to achieve fast diffusion. The PDMS chips were assembled to be three layer that one piece of polyvinylidene chloride (PVDC) membrane was embedded in two PDMS layers[7].

Gas concentration inside observation chamber was detected by adding 1mg/mL Ruthenium tris (2,2'-bipyridil) dichloride hexahydrate (RTDP, sigma). When two gas supply channels were fed with the same gas, the gas in observation window was kept homogeneous. Alternatively, when gas supply channels fed with two different kinds of gas, gas gradient can be established in observation window. In our experiment two kinds of gas conditions were established, homogeneous N2 and gas gradient of 1.75%-19.25% O2.

SI results

Details of the three-states swimming pattern. Three states can be distinguished statistically. For WT cell under control condition, the average value of instantaneous speed for run, reverse and tumble is (36.08±11.59) μm/s, (18.03±10.01) μm/s and (8.17±5.44) μm/s respectively. The correspondence average value of motion time is (3.25±3.77) s, (0.53±0.36) s and (0.10±0.09) s. Therefore, episodes of each state display significant differences on the mean speed - motion time 2D plot (Fig. S12).

The directional change within 0.05s is 97.43±55.53° during tumble, indicating the special property of tumble beside extreme low speed is continuous changing of

direction. Comparatively, the average value angular velocity in each episode of run and reverse is 34.61 °/s and 37.91 °/s respectively. Considering the AMB-1 can be treated as rod shape, with long axis a~2.5μm, short axis b~0.5 μm, the rotational diffusion is calculated to be $D_r=k_BT*(\ln(2a/b)-0.5)/8\pi\eta a^3/3)$, considering 2D focus, the average rotational diffusion angle $<\theta>=\mathrm{sqrt}(4D_rt)=30.61$ °/s, which is in consistency with the experimental results of run and reverse.

Considering the swimming of bacteria, translational diffusion effect can be evaluated as $D_{Trans}=\frac{s^2}{3(1-\alpha)\tau}$ where the displacement of cell under time interval τ is *s*, and α is the cosine of the mean angle between successive runs[8]. Therefore, larger speed induced more translational diffusional constant.

The angular shift of run-(tumble)-reverse, reverse-(tumble)-run and run-tumble-run is plotted in Fig. S13, with average value of (137.18±44.57) °, (128.30±51.71) ° and (35.33±42.50) °. We did not observed reverse-tumble-reverse event in control experiments. Under 1.0mT external magnetic field cells behave reverse-tumble-reverse with a low probability.

The handness and CW/CCW bias of AMB-1. The swimming pattern of amphitrichous flagellated bacteria is never investigated before, and we failed to stain AMB-1flagella. Therefore, dynamic coupling of flagella with swimming pattern is not provided by experiment but by reasonable deduction from other organism. Previous flagella model from peritrichous *Escherichia coli* and monotrichous *Vibrio alginolyticus* are well studied, both of which use the reversion of motor to adjust motility state. In *E. coli*, a set of flagella forms a bundle when motor runs in the counterclockwise (CCW) direction. The bundle dispersed when one or more motors turns clockwisely (CW). Chemotaxis is conducted by modulating the bias of CCW and CW[9]. Similarly, in *V. alginolyticus*, the CCW rotated motor push the cell forward while reversed motor pull the cell backward. Between reverse and run are flicks[10]. Motor switch change the motility status in both bacteria. Therefore, we deduced that

the changes between three motion states are the result from alteration of motor rotation. Whether the two flagella form bundle is unknown, but does not affect any conclusion in this paper.

The handness of bacteria can be obtained by observing swimming path near surface[11]. In our experiment, we found (1) the smooth-swimming bacteria moved in a CCW direction at the lower surface of the chamber and in a CW direction at the upper surface because of the frictional dragging force near surface. (2) Tethered bacteria rotate CW direction. Both observations are in agreement with the character of right-handed bacteria (Fig. S14)[11]. Therefore, it is plausible that AMB-1 perform run when both flagella rotate CW, while reverse when both flagella rotate CCW.

Compared to other bacteria also using motor reversal to change direction, *Vibrio alginolyticus* have a sequential run-reverse-tumble pattern with comparable motion time in runs and reverses[10], and *E. coli* maintain two-state stochastic switch between runs and tumbles[12]. Comparatively AMB-1 cells have larger translational speed and longer swimming intervals at run state (Fig. 2A-D), and the switch between the three states are randomly. These combinatorial properties in AMB-1 show the swimming pattern of amphitrichous flagellated bacteria is mixture of monotrichously and peritrichously flagellated bacteria.

Aerotactic behavior of AMB-1. We established a stable air gradient on-chip by constant injecting air and N2 to gas channel respectively. In this way oxygen concentration is linear distributed between two gas channels, with the concentration range of 1.75%-19.25% in observation area (Fig. S9B). WT and two knockout strains, Δ*amb0994-0995* and Δ*amb2196* were placed under air gradient and the position of ~100 cells was marked to calculate the population distribution (Fig. S8). All strains peaked at the oxygen concentration of 1.75% and maintained the same distribution. This result suggests WT, Δ*amb0994-0995* and Δ*amb2196* strains have the same aerotaxis behavior and deletion of *amb0995* does not affect aerotactic behavior.

AMB-1 has at least three kinds of aerotaxis MCPs, Heme-MCP, PAS-MCP and Hemerythrin-MCP. Each kind has more than one proteins. The recessive phenotype of *amb0995* knockout strain suggest other aerotactic MCP still function after deletion of PAS domain containing *amb0995*.

Supplementary table

Table S1. Primers used in this study

Number	Primer sequence from 5' to 3'	Use
1	ATTGGGCCCCACTTCGATGCGTCTGATCT	Cloning of upstream flank of *amb0994-0995*
2	CGCGGATCCAAACACGTCGTTGACGTAGGTC	
3	TGCTCTAGAGCGATTTTGGTTTTCAATGTGAAT	Cloning of downstream flank of *amb0994-0995*
4	CCCGAGCTCATGCCTTAAGAGTTTCATG	
5	GATAGGGCGATGTACTTGGCAA	Forward and reverse primers anchored in the chromosome for checking the deletion of *amb0994-0995*
6	ATGCGGCGTCCACCTACGATT	
7	ATTGGGCCCATTGGAGCCTTGCAACACAG	Cloning of internal fragment of *amb2196*
8	CCCGAGCTCGATGATCGCTGAGGAAACCG	
9	GGGGGTTGAAAATGGGTTTCA	Primers anchored in the chromosome for checking the insertion sites of *amb2196*
10	CGATTACGAGCTTGCTGCTCG	
11	CCGTAAAGCACTAAATCGGAAC	Forward and reverse primers anchored in the insertion plasmid
12	AGTGAGCGCAACGCAATTAAT	

Supplementary figures

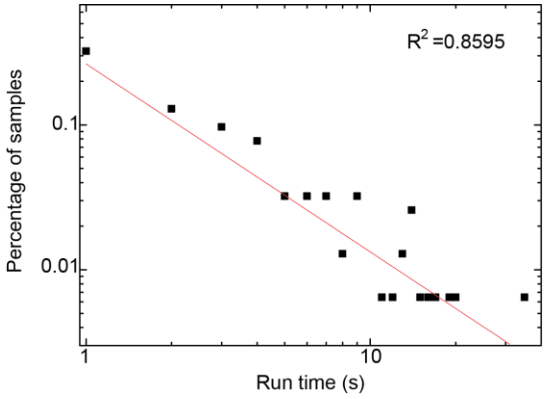

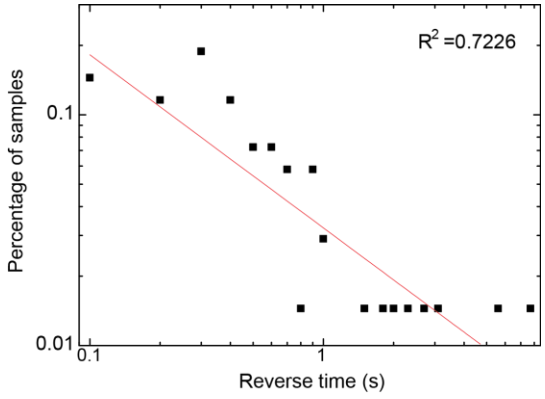

Fig. S1 log-log plot of run time and reverse time distribution in Fig.2F&G in main text.

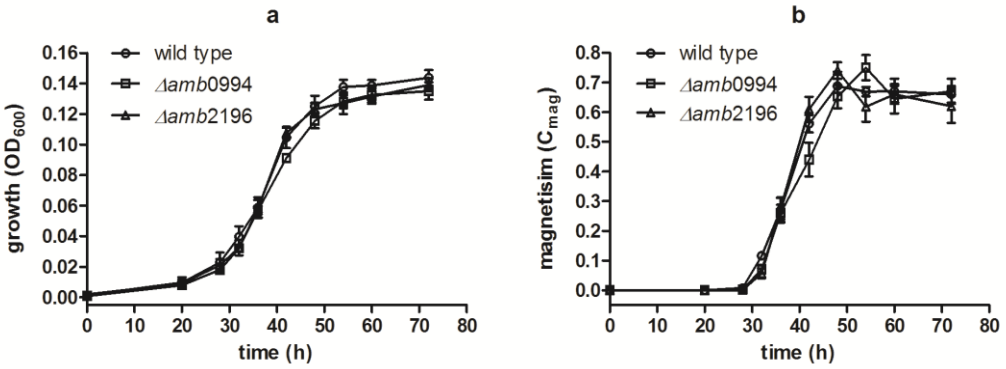

Fig. S2 Deletion of *amb0994* or *amb2196* in AMB-1 did not affect bacterial growth (OD600) and magnetism (C_{mag}). Growth curve (a) and corresponding C_{mag} value (b) of wild type and deletion mutant strains under microaerobic condition.

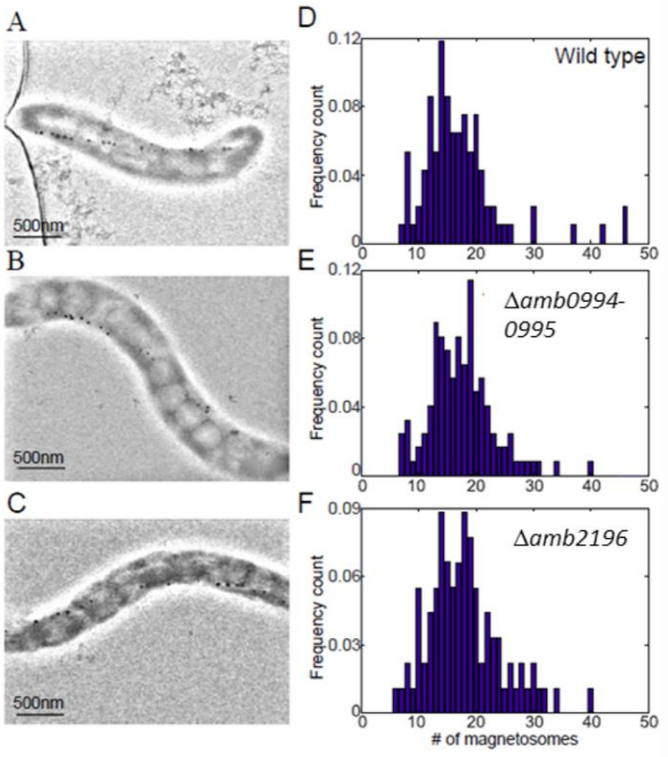

Fig. S3 Transmission electron microscopy (TEM) showed the well-arrangement of magnetosome chain (A-C) and the distribution of the number of magnetosomes in different strains (D-F). The number of magnetosomes in each cell was 17.1±7.1, 17.7±6.6, and 18.0±6.4 for WT, Δ*amb0994-0995* and Δ*amb2196* respectively. Each statistics includes 100 bacteria.

```
 Score =  738 bits (1904),  Expect = 0.0, Method: Compositional matrix adjust.
 Identities = 423/436 (97%), Positives = 430/436 (99%), Gaps = 0/436 (0%)

Query  1    METTLGSYARTLSLGMLVPSAICLLAGTFGLLGGSSIALWVVIAVSLLGVVGGVKIGGSA  60
            ME+TLGSYARTLSLGMLVPSAICLLAGTFGLLGGSSIALWVVI VSL+GVVGGVKIGGSA
Sbjct  1    MESTLGSYARTLSLGMLVPSAICLLAGTFGLLGGSSIALWVVITVSLIGVVGGVKIGGSA  60

Query  61   RRMAGDLSTAIHVLSRSASGDLNARILDVRGSGGIGALQHSINRLLDLAEAFGKEAFAAV  120
            RRMAGDLSTAIHVLSRSASGDLNARILDVRGS GIGALQ SINRLLDLAEAFGKEAFAAV
Sbjct  61   RRMAGDLSTAIHVLSRSASGDLNARILDVRGSDGIGALQRSINRLLDLAEAFGKEAFAAV  120

Query  121  ESANHGRYYRRIITTGLRGDFVLYAKTINQALKRMEARDAEFIAFANNQVKPVVNAVAAA  180
            ESANHGRYYRRIITTGLRGDFVLYAKTIN ALKRMEARDAEFIAFANNQVKPVVNAVAAA
Sbjct  121  ESANHGRYYRRIITTGLRGDFVLYAKTINHALKRMEARDAEFIAFANNQVKPVVNAVAAA  180

Query  181  ATELEASSGAMSAQSTDTSHQAMTVAAAAEQASVNVQAVASAVEEFSASIKEISTQVHRA  240
            ATELEASSGAMSAQSTDTSHQAMTVAAAAEQASVNVQAVASAVEEFSASIKEIS QVHRA
Sbjct  181  ATELEASSGAMSAQSTDTSHQAMTVAAAAEQASVNVQAVASAVEEFSASIKEISAQVHRA  240

Query  241  AAVASEAAGVASRTDTTVHGLSDAAQRIGAIVSLINDIAAQTNLLALNATIEAARAGDAG  300
            AAVASEAAGVASRTDTTVHGL++AA+RIGAIVSLINDIAAQTNLLALNATIEAARAGDAG
Sbjct  241  AAVASEAAGVASRTDTTVHGLNEAAERIGAIVSLINDIAAQTNLLALNATIEAARAGDAG  300

Query  301  KGFAVVANEVKNLANQTARATEDITSQVAHIQEVAAEAIKAIQEITRTVSQIEETSSAVA  360
            KGFAVVANEVKNLANQTARATEDITSQVAHIQ+VAAEAI+AI EITRTVSQIEETSSAVA
Sbjct  301  KGFAVVANEVKNLANQTARATEDITSQVAHIQQVAAEAIQAIDEITRTVSQIEETSSAVA  360

Query  361  GAVEEQNAVTVEIARNVAEAATGTSSVSSAIITVQATAAEATESAGQVADAASELSRQSE  420
            GAVEEQNAVTVEIARNVAEAATGTSSVSSAIITVQATAAEATESAGQVADAASELSRQSE
Sbjct  361  GAVEEQNAVTVEIARNVAEAATGTSSVSSAIITVQATAAEATESAGQVADAASELSRQSE  420

Query  421  NLSREVDGFIARIGGR  436
            NLSREVDGFIARIGGR
Sbjct  421  NLSREVDGFIARIGGR  436
```

Fig. S4 The blast result of Amb0994 and Amb2196. Amb2196 shares highest similarity among all AMB-1 proteins, which is 97% at protein level.

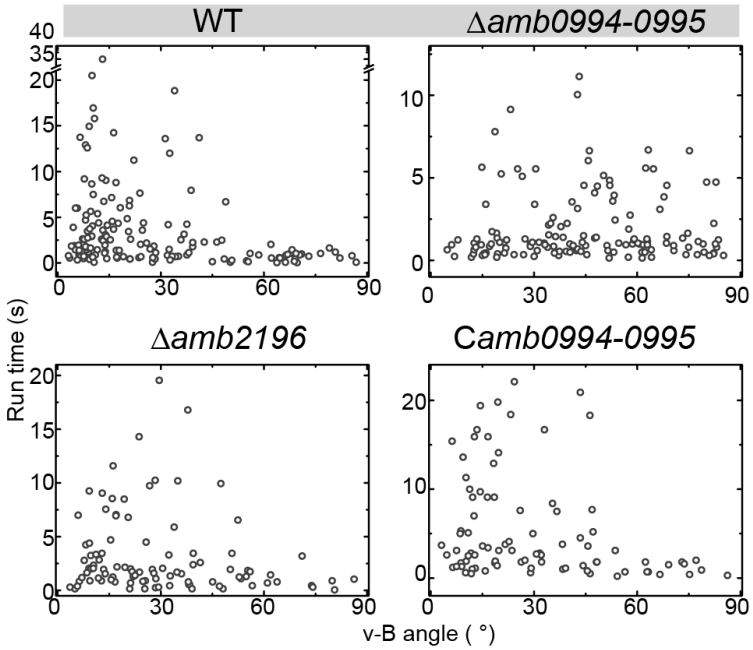

Fig. S5 Scatter plot of run time vs mean v-B angle of each episode in different strains. Notice that the y-axis has different scales in subfigures.

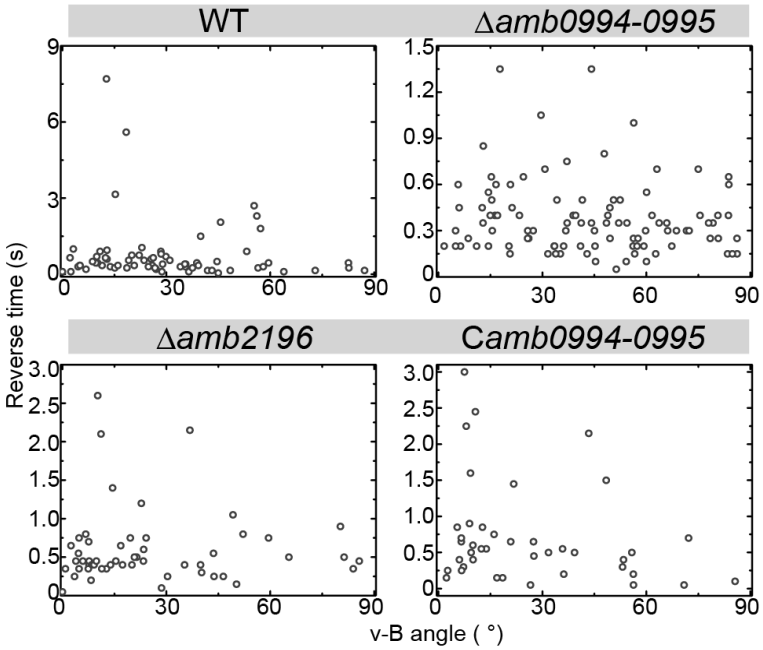

Fig. S6 Scatter plot of reverse time vs mean v-B angle of each episode in different strains. Notice that the y-axis has different scales in subfigures.

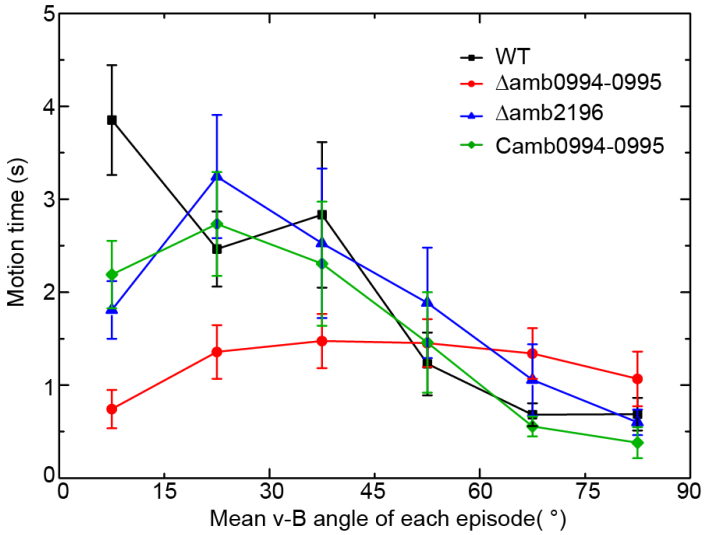

Fig. S7 The correlation between the overall motion and the v-B angle. Run states and reverse states are not distinguished here.

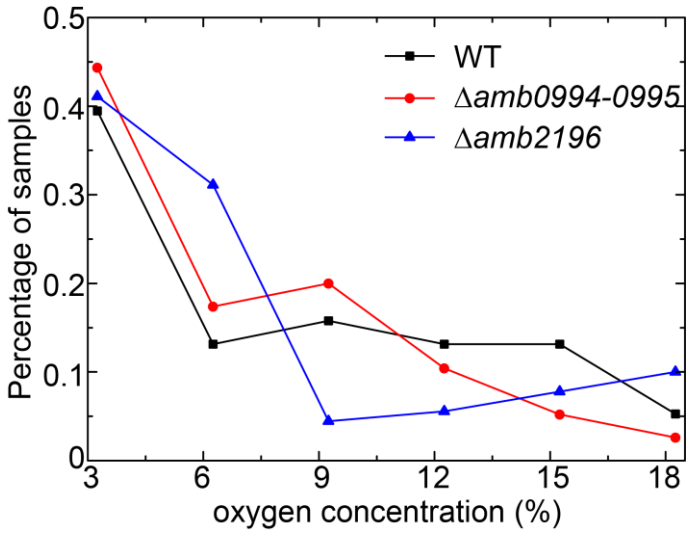

Fig. S8 The bacteria distribution under oxygen gradient.

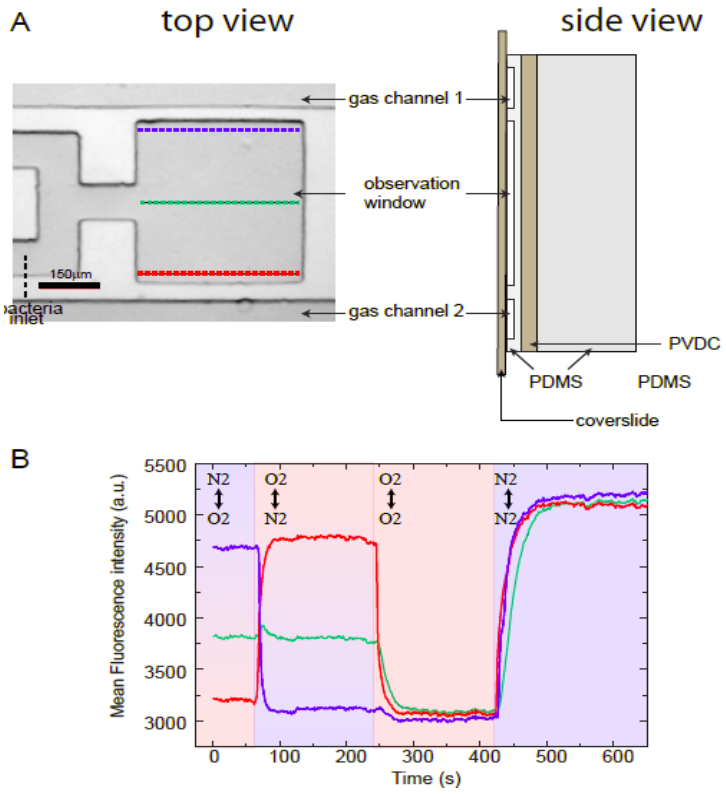

Fig. S9 Microfluidic setup and oxygen concentration calibration. (A) Top and side view of the device. Calibration was done by measuring the mean fluorescence intensity of three locations in observation area: 7.2 ±4.0μm from window boundary near gas channel1 (blue line); 7.2 ±4.0μm from window boundary near gas channel2 (red line) and 200.0±4.0μm from either boundary (green line). (B) The fluorescence intensity of RTDP due to oxygen quenching. Gases fed were marked by different

colors: N2 and O2 were highlighted at background by blue and red respectively.

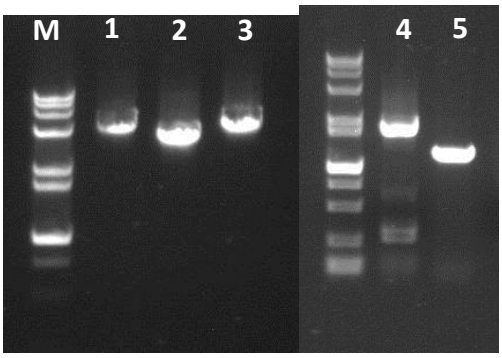

Fig.S10 Confirmation of target disruption of *amb0994-0995* and *amb2196*. Lane 1-3: PCR results using anchored primer F (upstream of amb0995) and R (downstream of amb0994) for wild type, Δ*amb0994-0995* and Δ*amb2196* strains to check the deletion of *amb0994-0995*. Lane 4 and 5: PCR results using anchored primer in upstream of *amb2196* on chromosome and primer in insertion plasimid, and downstream of *amb2196* on chromosome and primer in insertion plasmid for Δ*amb2196* strain.

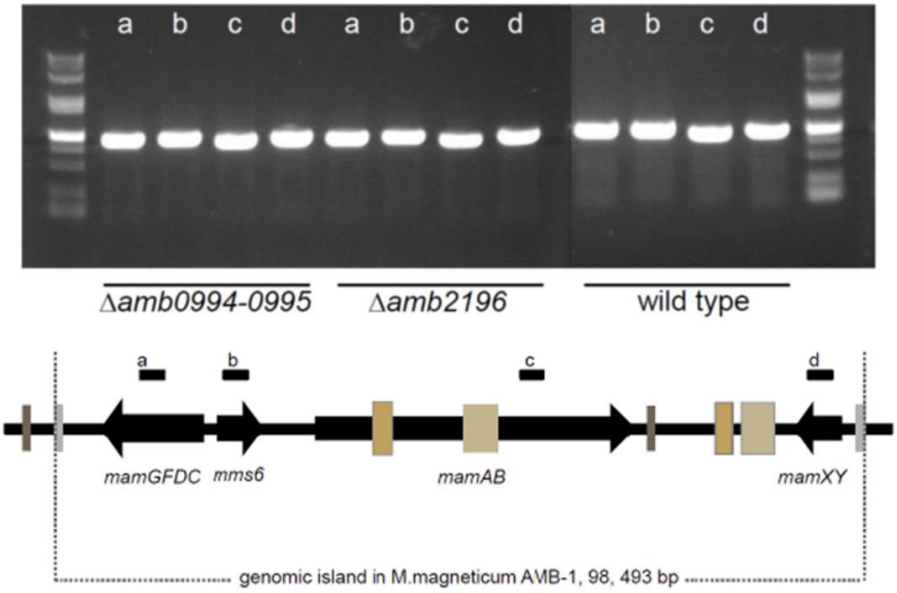

Fig. S11 Four segments within MAI were amplified to testify the maintenance of genomic MAI during deletion. The four segments (a-d) were chosen as denoted in[1].

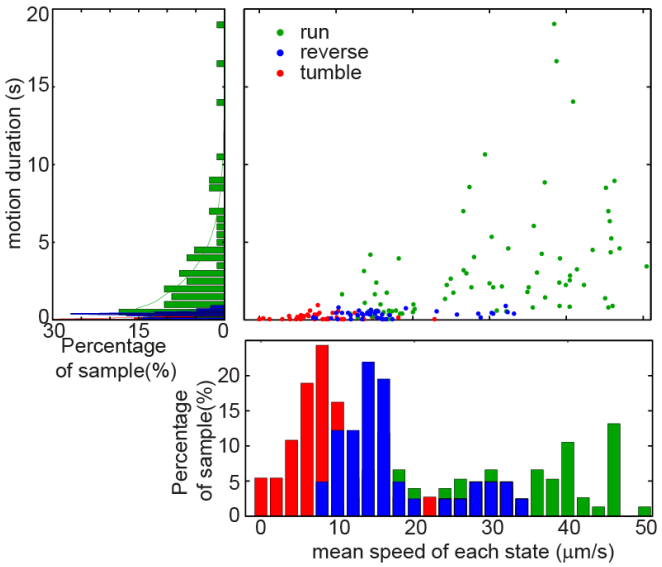

Fig. S12 Scatter of motion duration as a function of velocity for each state and the corresponding margin distribution for motion time and velocity of each episode. All data were collected from WT control condition.

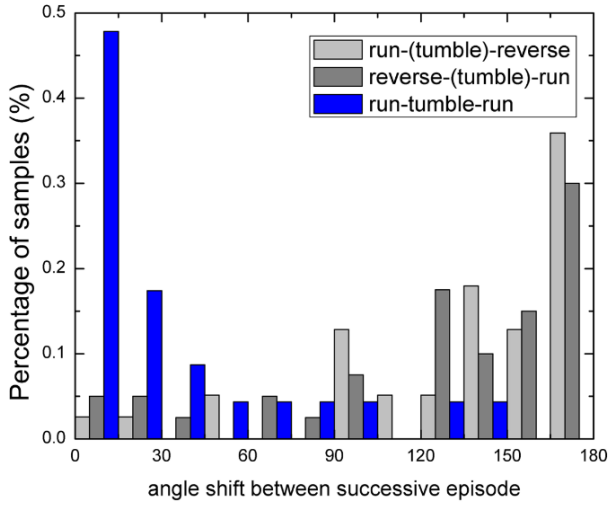

Fig. S13 The angular shift of three types of transition. The transition from reverse to reverse was not observed in experiment of WT under control condition.

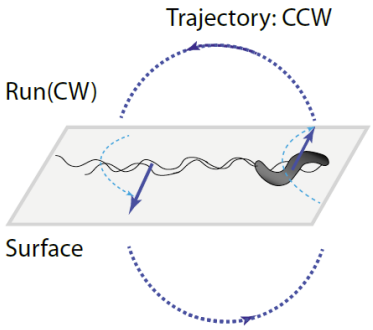

Fig. S14 A schematic drawing illustrating the swimming of a cell above a surface. The light blue curved arrows indicate the rotation directions of the cell body and flagella filament, and the straight arrows indicate the net lateral drag forces on them. The dashed dark blue arrow depicts the circular trajectory (derived from[13]).

SI movie

Time-lapse movie of AMB-1 motion. Here the objective lens is 100X, while time resolution is 0.05s.

SI References

1. X. Ge, K. Wang, T. Bo, Y. Kou, W. Liu, and G. Chen, *FEMS microbiology letters*, 2011, **320**, 118–27.

2. K. Wang, X. Ge, T. Bo, Q. Chen, G. Chen, and W. Liu, *Letters in applied microbiology*, 2011, **53**, 55–62.

3. J. H. Li, X. Ge, X. K. Zhang, G. J. Chen, and Y. X. Pan, *Chinese Journal Of Oceanology And Limnology*, 2010, **28**, 826–831.

4. C.-D. Yang, H. Takeyama, T. Tanaka, and T. Matsunaga, *Enzyme and Microbial Technology*, 2001, **29**, 13–19.

5. J.-B. Sun, F. Zhao, T. Tang, W. Jiang, J. Tian, Y. Li, and J.-L. Li, *Applied microbiology and biotechnology*, 2008, **79**, 389–97.

6. D. Schüler, R. Uhl, and E. Bäuerlein, *FEMS Microbiology Letters*, 1995, **132**, 139–145.

7. N. Li, C. Luo, X. Zhu, Y. Chen, Q. Ouyang, and L. Zhou, *Microelectronic Engineering*, 2011, **88**, 1698–1701.

8. P. S. Lovely and F. W. Dahlquist, *Journal of Theoretical Biology*, 1975, **50**, 477–496.

9. P. D. Frymier, R. M. Ford, H. C. Berg, and P. T. Cummings, *Proceedings of the National Academy of Sciences of the United States of America*, 1995, **92**, 6195–6199.

10. L. Xie, T. Altindal, S. Chattopadhyay, and X.-L. L. Wu, *Proceedings of the National Academy of Sciences of the United States of America*, 2011, **108**, 2246–2251.

11. B. L. Taylor and D. E. Koshland, *Journal of bacteriology*, 1974, **119**, 640–2.

12. H. C. Berg and D. A. Brown, *Nature*, 1972, **239**, 500–504.

13. G. Li, L.-K. K. Tam, and J. X. Tang, *Proceedings of the National Academy of Sciences of the United States of America*, 2008, **105**, 18355–18359.